DYNAMIC PERFORMANCE INFLUENCES ON HOPF BIFURCATION CHARACTERISTICS FOR VEHICLES

Haiyan Zhu[1,2], Pingbo Wu[1], Jing Zeng[1] and Guoyao Mai[1]

[1]Southwest Jiaotong University, State Key Laboratory of Traction Power, Chengdu 610031, Sichuan, China

[2]School of Railway Tracks and Transportation of East China Jiaotong University, Nanchang 330013, Jiangxi,China

Emails:zhupetrelcao@163.com,wupingb@163.com,

holdconquer@163.com,bessie2310@163.com

Submitted: Apr. 14, 2015 ***Accepted: July 12, 2015*** ***Published: Sep. 1, 2015***

Abstract- This study compares the performance influences for four kinds of tread contour features commonly used in High-Speed trains. The Hopf bifurcation characteristic influencing the dynamic performance for VEHICLE 1 and VEHICLE 2 were analyzed using mathematical matrices models. SIMPACK software was used to create two dynamic models for VEHICLE 1 and VEHICLE 2 for high speed trains equipped with four kinds of treads matched with Chinese 60 rail. Dynamic performance indices for these models were studied during operation in straight track conditions with imposed high interference German track irregularity spectra with the premise of dynamic performance normalized indices processing. The study shows that: VEHICLE 1 exhibits a subcritical bifurcation characteristic under different wheel-rail matching conditions. VEHICLE 2 dynamic performance index values do not increase as speed increases, but wear index gradually increased with increased speed. Vehicles with different structural parameters, wheel-rail matching greatly influences bifurcation stability, comfort and wheel-rail wear. This method indicates an important reference value for wheel-rail matching in high-speed trains and structural parameters of stability and safety for these vehicle systems.

Index terms: Hopf bifurcation characteristics, tread, stability and comfort, wheel-rail matching, dynamic performan

I. INTRODUCTION

Wheel-rail matching is a key technology for the safe operation of railway vehicles. With changes in vehicle speed or wheel-rail profile change, the wheel-rail forces produce a significant change which can affect the dynamic performance indices of such vehicles. Wheel-rail profile matching relationships involve the operational qualities and dynamic performance of high-speed trains. Wheel-rail interaction, surface wear and traction forces are always regarded as important technological study topics for high-speed trains, both in China and abroad.

Wen FangYu scholars[1] established the finite element model (FEM) spatial model of the wheel with the LMA tread profile and point rails of No. 38 high-speed turnout frog with the help of Software ANSYS-DYNA. And then the wheel-turnout contact states and dynamic characteristics were studied corresponding to forward and backward movements of wheels passing frogs. In addition, the influence of different lateral wheel displacements on wheel-rail contacts was investigated by analysis on the wheel center height, contact position and area and dynamic changes of vertical and lateral wheel-rail contact forces. Braghin[2] developed a wheel wear prediction model based on a multi-body code dynamic railway simulations. He employed a CONTACT 93 algorithm formulated by Kalker[3] to solve the non-Hertzian normal contact problem and the tangential problem, and used a local wear model that assumed direct proportionality between material removed and work done at the wheel–rail interface. Tao Gongquan scholars[4] set up the vehicle system dynamic model of 25G passenger car equipped with 209P bogie. The creep wheel/rail creep force and wheel/rail contact are analyzed when the passenger car operating on three typical curved tracks, in which the measured profiles of the wheels and rails from the sites are used. The obtained results indicate that the total creep force on the wheel of leading wheel set on the low rail of a curved track points to the third quadrant of the Cartesian coordinate system when the vehicle passing over the curved track. And the frequently passing over the sharp curves is the main reason of cracking and shelling the wheel tread field side. Butt, W.A[5] explored the concept of designing a wheel-rail matching profile, when researching a method to design wheel type surfaces for a given rail profile design to achieve wheel-rail wear reduction. In order to study the dynamic detection and identification method of wheel tread flat of a railway vehicle, Li, Yifan and Lin, JianHui et al.[6] set up a

vehicle-track coupled dynamic model and a wheel flat model to calculate the vehicle dynamic response. The results showed that the proposed method can effectively identify wheel tread flat and the running speed has no effect on this method. The multi-body dynamic software named SIMPACK was adapted to set up a complete dynamics model of locomotives by Wang Dakui scholars[7]. The influence of wheel profiles in different abrasion stages on the dynamic performances of locomotives was simulated and analyzed to contrast the wheel profiles in different abrasion stages. Ref.[8]developed a similar model using a multi-body code genesis for dynamic railway vehicle simulations. Again, the local contact analysis was solved using the Hertz theory and FASTSIM. The contact model employed within the multi-body simulation found, at most, two contact points simulations for each wheel–rail pair. A numerical method for robust geometry optimization of railway crossings is presented by Pålsson, Björn A[9]. The robustness was achieved by optimizing the crossing geometry for a representative set of wheel profiles. As a basis for the optimization, a crossing geometry was created where rail cross-sectional profiles and longitudinal height profiles of both wing rails and crossing nose were parameterized. The research showed that small nonlinear height deviations from a linear longitudinal wing rail profile in the transition zone can reduce the objective compared to the nominal design. Dynamic vehicle simulations for specified mission tracks were performed by the mathematical train–track interaction model developed previously in Ref.[10].

Investigated vehicle-track systems often operate within a few degrees of freedom (DOFs).The system employed by Hoffmann[11], Zboinski and Dusza[12,13] has 18 DOFS, Wickens[14] system has 21 DOFs, and Kim and Seok's system[15] has 31 DOFs. Bifurcation analysis is seldom carried out for models with many DOFs, one of the authors in Ref.[16,17,18] presented a nonlinear wheel-rail contact model and real design as well as worn profile shapes. Railway rolling stock stability assessment incorporates the possibility of applying the stability analysis to large complex vehicle models operating under realistic conditions. This approach required a large number of computations, and involved a variety of wheel-rail conditions in Ref.[19].

This article involves the application of bifurcation characteristics in the study of dynamic performance for VEHICLE 1 and VEHICLE 2 high speed trains. Four kinds of treads, S1002G, LMA, XP55 and LM, matched with Chinese 60 rails are examined in this paper. The models for high-speed trains of VEHICLE 1 and VEHICLE 2 are established by dynamic SIMPACK software, and the performance indices of vehicles are studied using assorted wheel-rail matching

and structural parameters that are based on researching the Hopf bifurcation characteristics. This approach will provide basic theory and technical support for various dynamic performance design methods for high-speed trains.

This article is structured as follows. Section Ⅰ is the introduction of literature review, section Ⅱ identifies contour features for four tread types (S1002G, LMA, XP55 and LM), and establishes VEHICLE system dynamics models, and section Ⅲ analyzes the Hopf bifurcation characteristics of vehicle systems and simulation models, and proposes indices for vehicle dynamic performance, and our conclusions are presented in section Ⅳ.

II. AN EXAMINATION OF TREAD CONTOUR FEATURES

Figure 1 shows four types of wheel contours named S1002G, LMA, XP55 and LM. By analyzing this figure we obtained three results:

(1) The flange of S1002G tread is wider than the other three treads, so its wheel-rail clearance is minimal. When the wheel set lateral movement is small, the rolling radius difference of treads, the wheel-rail contact angle difference and the equivalent conicity will be increased.

(2) Inside a nominal rolling circle, the surface shapes of the LMA tread and S1002G tread are similar. Outside of the nominal rolling circle, the LMA tread surface shapes and XP55 tread are similar. The outside flange curves of the LMA tread are relatively flat, so the corresponding values for the rolling radius difference, contact angle difference, and equivalent conicity remain relatively small as is the wheel set lateral movement variation.

(3) The XP55 tread flange is slightly high, and the flange thickness is slightly narrower than the other three kinds of tread. On the outside of the nominal rolling circle, tread curves decline significantly, and the LM tread shape can be treated as some averaged form of the other three treads.

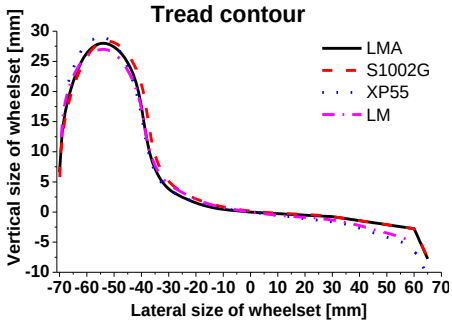

Figure 1. Contrast curve of the treads contour features

a. Establishment of VEHICLE system dynamics models

a.i Mathematical models

Differential equations for non-linear lateral motion for a four-axle vehicle were established in order to analyze lateral stability in the vehicle system. The equations only considered the lateral vibrations, and the lateral vibrations and the vertical vibrations do not coupling in the vehicle system. The models in Table.1 contain 7 rigid bodies which are: a vehicle body, two frames and four wheel sets for a total of 17 DOFs. Wheel sets and frames are connected by longitudinal, horizontal and vertical springs, and a vertical damper. The frames and vehicle body are connected by longitudinal, horizontal, vertical springs and three directions dampers.

Table1: DOFs of lateral vibration for a vehicle model

DOFs	Lateral movement	Rolling	Yaw
One vehicle body	1	1	1
Two frames	2	2	2
Four wheel sets	4	0	4

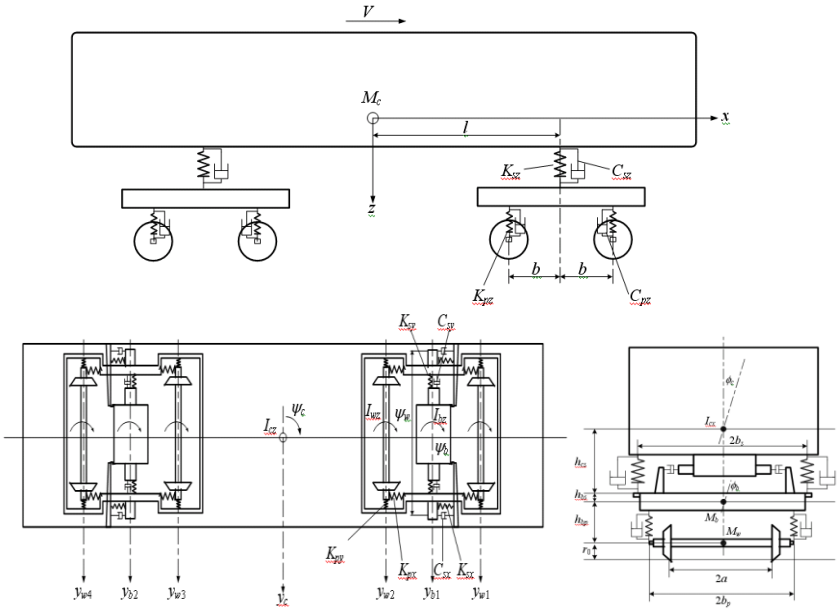

Figure 2. Lateral stability model for a vehicle

The 17 DOFs movement differential equations for calculating the vehicle lateral stability are as equations from (1) to (9), and these equations are used to calculate the lateral stability of the vehicle body. The meanings of all parameter symbols in the equations are described in the notation of Appendix.

Lateral movement of the vehicle body: equation (1) to calculate the lateral stability of lateral movement of the vehicle body.

$$\begin{aligned} &M_c y_c - 2K_{sy}\left(y_{b1}+_{b2} - h_{bs}\varphi_{b1} - h_{bs}\varphi_{b2} - 2h_{cs}\varphi_c - 2y_c\right) \\ &-2C_{sy}\left(y_{b1}+_{b2} - h_{bs}\varphi_{b1} - h_{bs}\varphi_{b2} - 2h_{cs}\varphi_c - 2y_c\right) = 0 \end{aligned} \tag{1}$$

Rolling of the vehicle body: equation (2) to calculate the lateral stability of rolling of the vehicle body.

$$\begin{aligned} &I_{cx}\varphi_c - 2h_{cs}K_{sy}\left(y_{b1}+y_{b2} - h_{bs}\varphi_{b1} - h_{bs}\varphi_{b2} - 2h_{cs}\varphi_c - 2y_c\right) \\ &-2h_{cs}C_{sy}\left(y_{b1}+y_{b2} - h_{bs}\varphi_{b1} - h_{bs}\varphi_{b2} - 2h_{cs}\varphi_c - 2y_c\right) \\ &-2d_s^2K_{sz}\left(\varphi_{b1}+\varphi_{b2}-2\varphi_c\right) - 2d_s^2C_{sz}\left(\varphi_{b1}+\varphi_{b2}-2\varphi_c\right) = 0 \end{aligned} \tag{2}$$

Yaw of the vehicle body: equation (3) to calculate the lateral stability of yaw movement of the vehicle body.

$$\begin{aligned} &I_{cs}\psi_c - 2lK_{sy}\left(y_{b1}-y_{b2}-2l\psi_c\right) - 2d_s^2K_{sx}\left(\psi_{b1}+\psi_{b2}-2\psi_c\right) \\ &-2lC_{sy}\left(y_{b1}-y_{b2}-2l\psi_c\right) + 2d_s\left(F_1+F_2\right) = 0 \end{aligned} \tag{3}$$

In which, $F_m = \begin{cases} \frac{F_0}{c_0}(\psi_c-\psi_{bm})d_s, & |\psi_c-\psi_{bm}|d_s \geq c_0 \\ \frac{F_0(\psi_c-\psi_{bm})d_s}{|\psi_c-\psi_{bm}|}, & |\psi_c-\psi_{bm}|d_s < c_0 \end{cases} (m=1,2)$

Lateral movement of the bogies: equation (4) to calculate the lateral stability of lateral movement of the bogies.

$$\begin{aligned} &M_b y_{bm} - 2K_{py}\left[y_{wn}+y_{w(n+1)}-2y_{bm}-2h_{bp}\varphi_{bm}\right] \\ &-2C_{py}\left[y_{wn}+y_{w(n+1)}-2h_{bp}\varphi_{bm}-2y_{bm}\right] - 2K_{sy}\left[y_c+h_{cs}\varphi_c-(-1)^m l\psi_c+2h_{bs}\varphi_{bm}-y_{bm}\right] \\ &-2C_{sy}\left[y_c+h_{cs}\varphi_c-(-1)^m l\psi_c-y_{bm}+2h_{bs}\varphi_{bm}\right] = 0 \\ &m(n) = 1(1), 2(3) \end{aligned} \tag{4}$$

Rolling of the bogies: equation (5) to calculate the lateral stability of rolling of the bogies.

$$\begin{aligned} &I_{bx}\varphi_{bm} - 2h_{bp}K_{py}\left[y_{wn}+y_{w(n+1)}-2y_{bm}-2h_{bp}\varphi_{bm}\right] - 2h_{bp}C_{py}\left[y_{wn}-2y_{bm}+y_{w(n+1)}-2h_{bp}\varphi_{bm}\right] \\ &+4d_p^2\left(K_{pz}\varphi_{bm}+C_{pz}\varphi_{bm}\right) - 2h_{bs}K_{sy}\left[y_{bm}-h_{bs}\varphi_{bm}-y_c-h_{cs}\varphi_c+(-1)^m l\psi_c\right] \\ &-2h_{bs}C_{sy}\left[y_{bm}-h_{bs}\varphi_{bm}-y_c-h_{cs}\varphi_c+(-1)^m l\psi_c\right] - 2d_s^2K_{sz}\left(\varphi_c-\varphi_{bm}\right) - 2d_s^2C_{sz}\left(\varphi_c-\varphi_{bm}\right) = 0 \\ &m(n) = 1(1), 2(3) \end{aligned} \tag{5}$$

Yaw of the bogies: equation (6) to calculate the lateral stability of yaw movement of the bogies.

$$\begin{aligned} &I_{bz}\psi_{bm} - 2d_p^2 K_{px}\left[\psi_{wn} + \psi_{w(n+1)} - 2\psi_{bm}\right] - 2d_p^2 C_{px}\left[\psi_{wn} + \psi_{w(n+1)}\right] - 2bK_{py}\left[y_{wn} - y_{w(n+1)} - 2b\psi_{bm}\right] \\ &-2bC_{py}\left[y_{wn} - y_{w(n+1)} - 2b\psi_{bm}\right] - 2d_s^2 K_{sx}\left(\psi_c - \psi_{bm}\right) - 2d_s F_m = 0 \\ &m(n) = 1(1), 2(3) \end{aligned} \tag{6}$$

Lateral movement of the wheel sets: equation (7) to calculate the lateral stability of lateral movement of the wheel sets.

$$\begin{aligned} &M_w y_{wn} - 2K_{py}\left[y_{bm} + h_{bp}\varphi_{bm} - (-1)^m b\psi_{bm} - y_{wn}\right] - 2C_{py}\left[y_{bm} + h_{bp}\varphi_{bm} - (-1)^m b\psi_{bm} - y_{wn}\right] - F_{latn} = 0 \\ &n(m) = 1(1), 2(1), 3(2), 4(2) \end{aligned} \tag{7}$$

Yaw of the wheel sets: equation (8) to calculate the lateral stability of yaw movement of the bogies.

$$\begin{aligned} &I_{wz}\psi_{wn} - 2d_p^2 K_{px}\left(\psi_{bm} - \psi_{wn}\right) - 2d_p^2 C_{px}\left(\psi_{bm} - \psi_{wn}\right) - M_{yawn} = 0 \\ &n(m) = 1(1), 2(1), 3(2), 4(2) \end{aligned} \tag{8}$$

In the differential equations above, the subscript m= 1, 2, represents the front and rear bogies, and the subscript n = 1, 2, 3, 4 denotes the first, second, third and fourth wheel sets. These equations can be expressed using the matrix below (9):

$$[M]\ddot{y} + [C]\dot{y} + [K]y = \{0\} \tag{9}$$

Where $[M]$、$[C]$ and $[K]$, respectively denote the inertia, damping and stiffness matrices for the vehicle system. $\ddot{y}$ 、 $\dot{y}$ and y denote vector variables for displacement, velocity and acceleration, and $\{0\}$ denotes the zero column vector. Therefore, data are presented in a 17×17 square matrix.

a.ii Hopf bifurcation characteristics of vehicle system

Hopf bifurcation refers to a critical bifurcation parameter value, and the equilibrium point of the system becomes unstable, and generates the limit cycle.

The Hopf bifurcation consists of supercritical and subcritical forms in the railway vehicle system (see Figure 3). Supercritical bifurcation refers to the limit cycle and the stable equilibrium point of the system distributed on two sides of the Hopf bifurcation. By contrast, the subcritical bifurcation of the system refers to the limit cycle and a stable equilibrium point found on the same side of the Hopf bifurcation. The solid lines represent a stable limit cycle, and the dotted lines represent a non-stable limit cycle. Point A is the Hopf bifurcation point, and the speed at

point A is called the linear critical velocity V_A. The speed at point D is called the nonlinear critical speed V_D. In actuality, if the vehicle speed exceeds the V_A, regardless of the type of vehicle bifurcation, the vehicle will generate a limit cycle movement.

For the supercritical bifurcation vehicle in Figure 3(a), when the critical speed V_A is exceeded, the maximum value of the limit cycle amplitude will gradually increase or decrease as speed increases or decreases. Therefore, it can be applied to a vehicle's early warning, control and protection of running safety, or unstable. In addition, the yaw unstable of vehicle has no relationship with the size of orbital excitation, and the corresponding Hopf bifurcation value is the only critical speed of the vehicle.

The subcritical bifurcation vehicle is shown in Figure 3(c). While vehicle speed is below V_D, the system remains absolutely stable. But when the speed exceeds V_A, the system suddenly generates a substantial limit cycle, when the speed is between V_D and V_A, the system stability is uncertain, and if the outside excitation is large, then the system is unstable. If the excitation is small, then the system is in convergence. When the speed exceeds V_D, and the vehicle system becomes unstable. Stability can be restored only when its speed is decreased to V_D. So, when the subcritical bifurcation unstable values for the vehicle are unpredictable and uncontrollable, then the instability consequences become very serious.

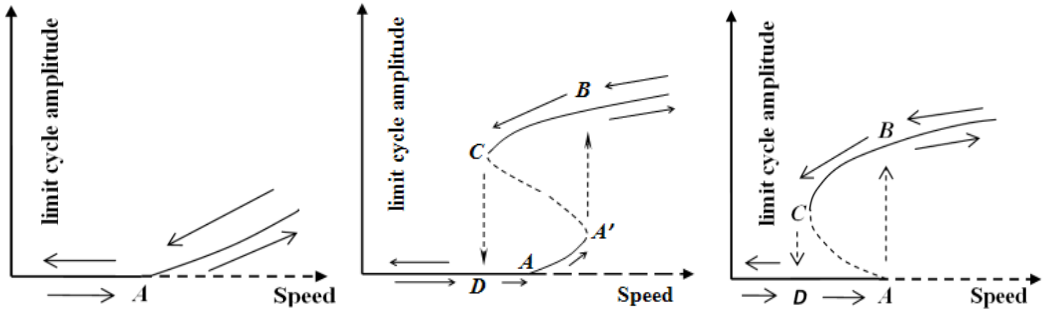

(a) Supercritical bifurcation. (b) Supcritical bifurcation. (c) Subcritical bifurcation.

Figure 3. Bifurcation forms of vehicle system

a.iii Simulation models

The dynamic parametric simulation models for high-speed trains of VEHICLE 1 and VEHICLE 2 were established using SIMPACK software. Each model contains 15 entities per vehicle body, two frames, four wheel sets, eight rotary arms, and the models have been simplified to depict rigid bodies. Each of vehicle bodies, bogie frames and wheel sets has 6 DOFs which include

longitudinal, horizontal and vertical displacements as well as roll, pitch and yaw rotations, and each rotary arms has got pitch rotation DOF. Therefore, one trailer section contains a total of 50 DOFs. Wheel sets are connected to the frames through primary suspension, and are equipped with vertical dampers and axle box rotary arm positioning devices. Frames are connected to the vehicle body using air springs equipped with anti-yaw dampers, and lateral and vertical damper parts. The vehicle part parameters of models are shown in Table.2, and the SIMPACK simulation models appear in Figure 4.

Table 2: The VEHICLES part parameters of models

Parameters	**VEHICLE 1**	**VEHICLE 2**	**Units**
$2b$	17500	17375	mm
$2l$	2500	2500	mm
$2r_0$	860	920	mm
$2a$	1353	1353	mm
M_c	35.88	36.82	t
I_{cx}	116.25	119.28	t m^2
I_{cy}	1758.12	1803.94	t m^2
I_{cz}	1659.09	1702.33	t m^2
H_c	1.52	1.656	m
M_b	3.12	2.2	t
I_{bx}	2.527	1.236	t m^2
I_{by}	1.709	1.233	t m^2
I_{bz}	3.120	2.336	t m^2
H_b	0.51	0.574	m
M_w	1.7518	1.517	t
I_{wx}	0.631	0.693	t m^2
I_{wy}	0.070	0.118	t m^2
I_{wz}	0.631	0.693	t m^2
M_{zb}	0.0482	0.0667	t
I_{zbx}	0.0007	0.0003	t m^2
I_{zby}	0.0028	0.0020	t m^2
I_{zbz}	0.0026	0.0020	t m^2

III. COMPARISION OF DYNAMIC PERFORMNCES FOR VEHICLE 1 AND VEHICLE 2

Four kinds of treads, LMA, XP55, LM and S1002G, were installed in the VEHICLE 1 and VEHICLE 2 models, and matched with 60Kg/m rails. The two models were tested using

simulations for straight track running conditions with track's irregularity high interference German spectra in order to analyze dependence between indices of vehicle dynamic performance and Hopf bifurcation characteristics. The test include studies of: lateral stability, vertical stability, comfort, and maximum indices of wheel set lateral force, vertical wheel-rail force, derailment coefficients, wheel load reduction rates, lateral acceleration of frames, and wear indices.

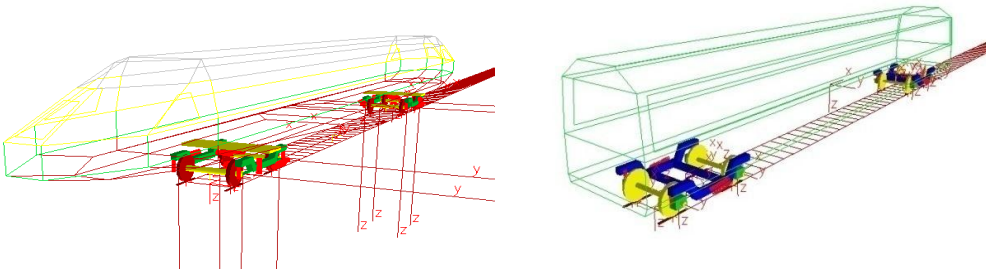

(a) Trailer model of VEHICLE 1 (b) Trailer model of VEHICLE 2

Figure 4. Structure of the VEHICLES' nominal models adopted in SIMPACK software

During the simulation and calculation processes, stability, comfort and safety indices were processed using the normalization method with the rules as follows. A value for the stability and comfort index of "1" denotes an excellent limit value, which main refers to the lateral stability index, vertical stability index and comfort index and so on. And a value for the safety index of "1" denotes a safety limit value, which main refers to the derailment coefficient, wheel-rails vertical force, rate of wheels load reduction and derailment coefficient and so on.

a. Comparison analysis of stability and comfort

For the VEHICLE 1 original structural parameters, the system exhibits a subcritical bifurcation characteristic under different wheel-rail matching conditions. When vehicle speed exceeds the nonlinear critical speed of the subcritical bifurcation V_n, the lateral stability index increases rapidly (see Figure 5(a)). So, when vehicle speed exceeds the nonlinear critical speed, the system generates lateral unstable under the actual line spectrum excitation, and the vehicle's comfort balance is seriously influenced. Therefore, in order to ensure safety and comfort in vehicles with sharp subcritical bifurcation characteristics, speeds should be not exceeded the nonlinear critical speed V_n. For the VEHICLE 2 original structural parameters, and low conicity LMA and XP55

treads, the vehicle body's first resonance frequency easily coincides with the low frequency yaw of the wheel set, and produces resonance. Therefore, the vehicle stability and comfort is comparatively poor (see Figure 5, Figure 6(b) and Figure 7(b)). If LM and S1002G high conicity treads are used, the vehicle's stability and comfort performance will be excellent, and stability and comfort indices do not rapidly increase as the speed increases. So, this can ensure the vehicle's overall operational comfort for passengers.

Considering these two models, stability and comfort are comparatively poor if the vehicle's wheel-rail matching has significantly unstable characteristics. By contrast, if vehicle wheel-rail matching has significantly stable characteristics, then the stability and comfort values are excellent.

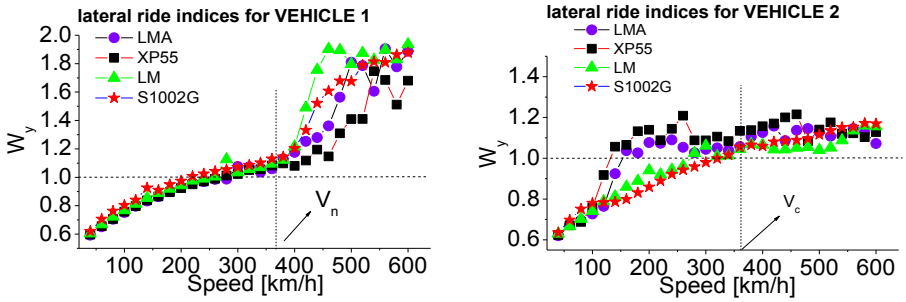

(a) VEHICLE 1 (b) VEHICLE 2

Figure 5. Normalized values of lateral ride indices for VEHICLE 1 and VEHICLE 2 with different wheel-rail matching

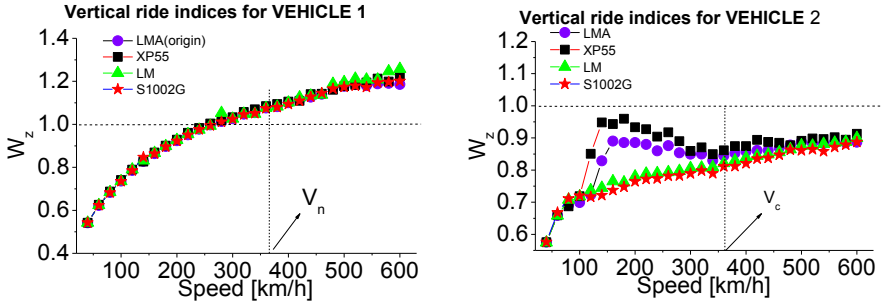

(a) VEHICLE 1 (b) VEHICLE 2

Figure 6. Normalized values of vertical stability indices for VEHICLE 1 and VEHICLE 2 with different wheel-rail matching

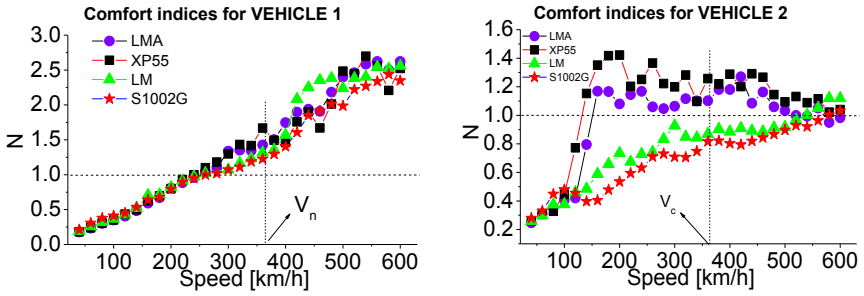

(a) VEHICLE 1 (b) VEHICLE 2

Figure 7. Normalized values of comfort indices for VEHICLE 1 and VEHICLE 2 with different wheel-rail matching

For VEHICLE 1 original structural parameters, if LMA and XP55 is applied using low conicity treads, the result will be excellent safety performance. While vehicle speed remains below nonlinear critical speed V_n, various indices will be safe. If vehicle speed exceeds nonlinear critical speed V_n, all safety index values will increase rapidly, and exceed the safety limit. Therefore, subcritical bifurcation is not conducive to monitoring a vehicle's operational safety. For vehicles exhibiting subcritical bifurcation operational safety can only be ensured, when their speed remains below the nonlinear critical speed V_n.

For VEHICLE 2 original structural parameters, if applied to LMA and XP55 with high conicity treads, the results show excellent dynamic performance, (see Figure 12(b)).

When speed exceeds the Hopf bifurcation point (V_c) and VEHICLE 2 is matched with tread S1002G or LM, then either vehicle's frame lateral acceleration curve slope decreased significantly, or vehicle's lateral unstable process was reduced, which requires monitoring vehicle's unstable status. If VEHICLE 2 applied to LMA and XP55 with low conicity treads, then both lateral wheel set force and the derailment coefficients both fluctuate significantly. This happens because of applying low conicity treads (LMA, XP55) to VEHICLE 2 produces a subcritical bifurcation, and causes significant lateral yaw unstable values. For the four kinds of wheel-rail matching, VEHICLE 2 safety performances are excellent. Except for a rapidly increasing derailment coefficient during high-speed operation, the remaining safety indices increased gradually with increasing speed, even when the speed exceeded the Hopf bifurcation point. Each index value has no mutation.

Based on the above analysis, which can be concluded that wheel set selection obviously impacts

bifurcation stability and comfort for vehicles with different structural parameters, but could not play a decisive role in vehicle safety. However, the vehicle's suspension parameters can play a decisive role in affecting safety index trends.

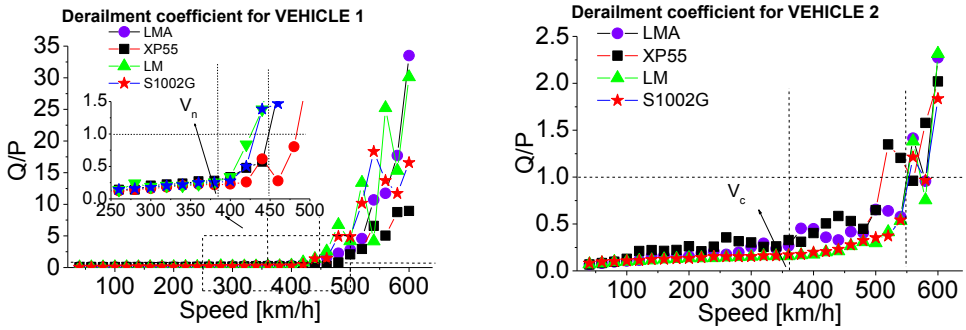

(a) VEHICLE 1 (b) VEHICLE 2

Figure 8. Normalized values of maximum derailment coefficient for VEHICLE 1 and VEHICLE 2 with different wheel-rail matching

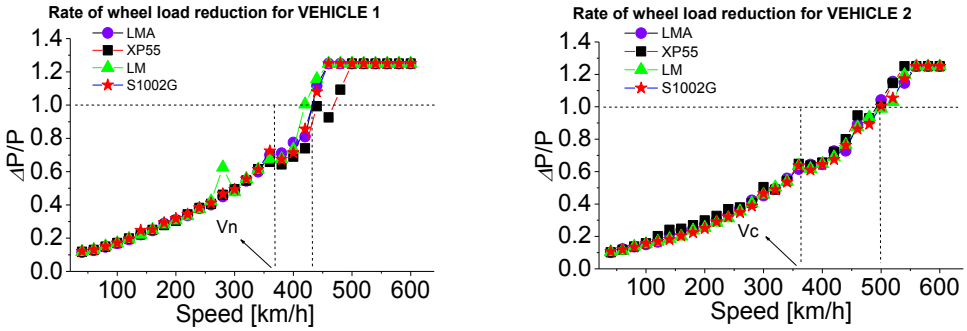

(a) VEHICLE 1 (b) VEHICLE 2

Figure 9. Normalized values of maximum rate of wheel load reduction for VEHICLE 1 and VEHICLE 2 with different wheel-rail matching

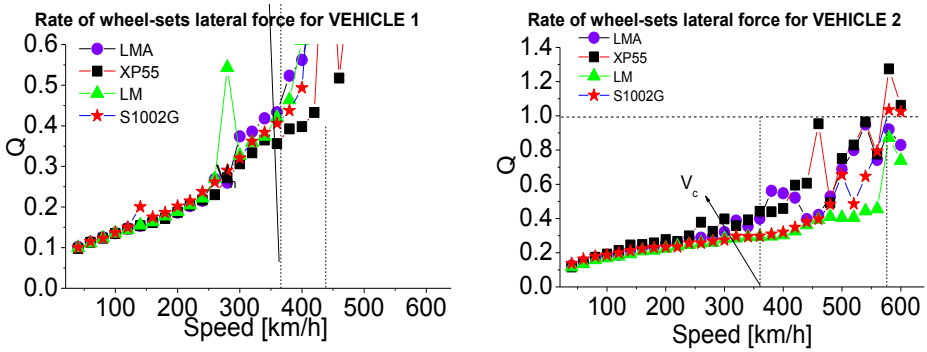

(a) VEHICLE 1 (b) VEHICLE 2

Figure 10. Normalized values of maximum rate of wheel-axe lateral force for VEHICLE 1 and VEHICLE 2 with different wheel-rail matching

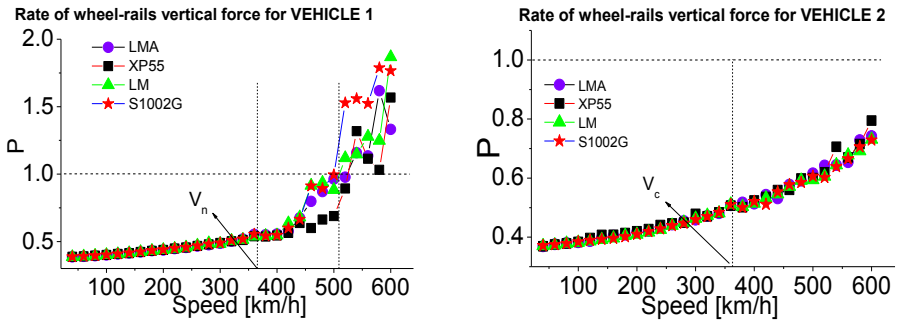

(a) VEHICLE 1 (b) VEHICLE 2

Figure 11. Normalized values of maximum rate of wheel-rail vertical force for VEHICLE 1 and VEHICLE 2 with different wheel-rail matching

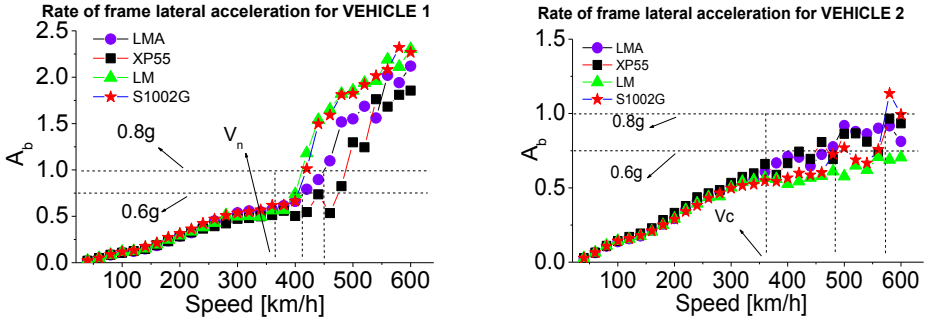

(a) VEHICLE 1 (b) VEHICLE 2

Figure 12. Normalized values of maximum rate of frames lateral acceleration for VEHICLE 1 and VEHICLE 2 with different wheel-rail matching

b. Contrast of wheel-rail wear indices

For VEHICLE 1 original structural parameters (see Figure 13(a)), when speed remains below system nonlinear critical speed V_n, the four wheel-rail wear index values are low. For VEHICLE 2 operating under the same conditions, wear index values are even lower. When speed exceeds nonlinear critical speed V_n, the wheel set generates a large yaw unstable value that is below the actual line spectrum excitation, thus causing a rapid increase in wear index. For the four kinds of

wheel-rails matching, the wear indices of low conicity treads LMA and XP55 are relatively low, while the wear indices for high conicity treads S1002G and LM are relatively high.

For the VEHICLE 2 original structural parameters, Figure 13 (b) indicates that: four types of wheel-rails wear index values are not high. The analysis shows that when VEHICLE 2 is applied the low conicity treads LMA and XP55, wheel sets will generate a large maximum value for yaw movement, and result in a relatively high wear index values for the two treads. When using high conicity treads S1002G and LM for VEHICLE 2, the maximum wheel set yaw values are not large, but wear indices increase gradually with increasing speed.

Based on the above analysis, a large maximum yaw value of the wheel set will increase wheel-rail wear, which not only affects high-speed trains' operational safety, but also increases maintenance costs. Therefore, measures should be employed to control maximum wheel set yaw values.

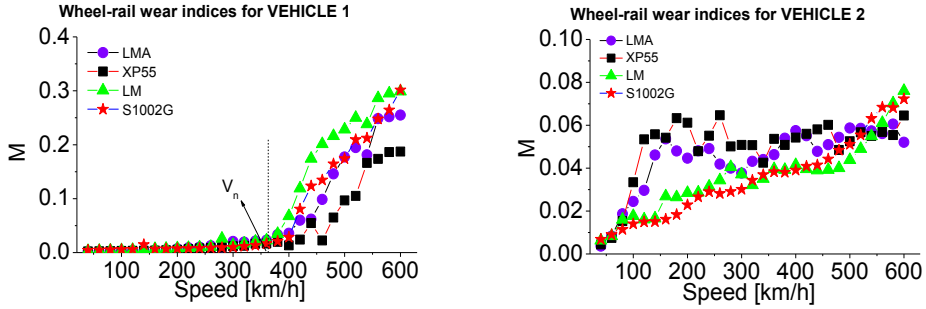

(a) VEHICLE 1 (b) VEHICLE 2

Figure 13. Normalized values of wheel-rail wear indices for VEHICLE 1 and VEHICLE 2 with different wheel-rail matching

IV. CONCLUSIONS

Mathematical matrices models are established and two dynamic models for high-speed trains of VEHICLE 1 and VEHICLE 2 were created by SIMPACK software in this paper. Dynamic performance indices for these models were studied during operation in straight track conditions with imposed high interference German track irregularity spectra with the premise of dynamic performance normalized indices processing. And the study results are as follows.

For VEHICLE 1 original structural parameters, the system exhibits subcritical bifurcation characteristic under different wheel-rail matching conditions. While vehicle speed remains

nonlinear critical speed V_n, stability, comfort and safety remain below the dynamic performance index values. Concurrently, the wheel-rail wear index value is low. When speed exceeds nonlinear critical speed V_n, the wheel set generates a large maximum yaw unstable value that remains below the actual line spectrum excitation which can reduce the stability, comfort and running safety, and cause wheel-rail wear indices to increase rapidly.

For VEHICLE 2 original structural parameters that are applied to low conicity treads, a large maximum value yaw unstable is generated, even while operating at low speed. This situation causes rather poor stability and comfort, and a high wheel-rail wear index. When using high conicity treads, the maximum value for wheel set yaw becomes lower, and vehicle stability and comfort is excellent. Moreover, dynamic performance index values could not increase with increasing speed, and values of stability, comfort and safety remain excellent. However, wear index values gradually increase with increasing speed.

For different vehicle structural parameters, wheel-rail matching greatly influences bifurcation stability, comfort and wheel-rail wear, but could not play a decisive role in vehicle safety. If the maximum value of wheel set unstable becomes larger, stability and comfort values decrease, and wheel-rail wear is accelerated. But the maximum unstable value has no direct correlation with vehicle safety.

V. ACKNOWLEDGEMENTS

The research presented in this article would not have been possible without a project subsidy from *the Key Technologies of Construction and Integration Design for Pedigree Module of High-Speed Train* (2012AA112001-02), and *Research the Limit Speed of High-Speed Train in Trains Coupling Conditions* (2011CB711106) and National Natural Science Fund of China (U1334206). The authors wish to thank the Traction Power State Key Laboratory (TPL) research group of Southwest Jiaotong University(SWJTU), for their participation this research.

REFERENCES

[1] Wen. Fangyu, Ren. Zunsong, and Sun. Shouguang, “ANSYS/DYNA-based study on wheel-rail dynamics of high-speed wheel-turnout system”, Journal of the China Railway Society, vol. 36,

no. 3, pp. 14-18, 2014.

[2] F. Braghin, S. Bruni and F. Resta, "Wear of railway wheel profiles: a comparison between experimental results and a mathematical model", Veh Syst Dyn, Vol. 37, No.1, pp. 478–489,2002.

[3] J.J. Kalker, "Three-Dimensional Elastic Bodies in Rolling Contact", Kluwer Academic Publisher, Dordrecht, 1990.

[4] Tao. Gongquan,Wang. Hengyu, Zhao. Xin, Du. Xing, Wen. Zefeng, Guo, Jun, Zhu, Minhao, "Research on wheel tread damage mechanism based on interaction of wheel and rail", Journal of Mechanical Engineering, Vol.49,No.18,pp. 23-29,September 20, 2013.

[5] Butt, W.A, "Observer based dynamic surface control of a hypersonic flight vehicle", International Journal on Smart Sensing and Intelligent Systems, vol.6, No.2, 2013, pp. 664-688.

[6] Li. Yifan, Lin. Jianhui, Liu. Jianxin, Wang. Kaiyun, Chen. Shuangxi, "Identification method of wheel tread flat, Journal of Vibration and Shock", Vol. 32, No. 22, pp. 21-27, 2013.

[7] Wang. DaKui , Zhang. Jun, Zhang. Xiujuan, Sheng. Youyi, "Dynamic performance analysis of locomotives based on the matching between worn wheel-rail", Advanced Materials Research, Vol. 748,No.5,pp. 386-389,2013.

[8] Aldair, A.A, Wang, W.J, "Design an intelligent controller for full vehicle nonlinear active suspension systems", International Journal on Smart Sensing and Intelligent Systems, vol.4, No.2, 2011, pp.224-243.

[9] Pålsson, Björn A, "Optimisation of railway crossing geometry considering a representative set of wheel profiles", Vehicle System Dynamics, Vol.53, No.2, pp. 274-301, February, 2015.

[10] S. Bruni, A. Collina and R. Corradi, "Numerical modeling of railway run ability and ballast settlement in railroad bridges", in: Proceedings of the EURODYN International Conference, 2002.

[11] Hoffmann, M, "On the Dynamics of European Two-Axle Rail way Freight Wagons", Nonlinear Dyn, Vol.52, No. 7, 2008,pp.301-311.

[12] Zboinski, K., and Dusza, M, "Bifurcation Approach to the Influence of Rolling Radius Modeling and Rail Inclination on the Stability of Railway Vehicles in a Curved Track", Veh Syst Dyn, Vol.46, No. 8,2008, pp.1023-1037.

[13] Zboinski, K., and Dusza, M, "Extended Study of Railway Vehicle Lateral Stability in a Curved Track", Veh Syst Dyn, Vol.49, No.5, 2011, pp.789-810.

[14] Wickens, A. H, "Comparative Stability of Bogie Vehicles With Passive And Active

Guidance as Influenced by Friction and Traction", Veh Syst Dyn, Vol.47, No.9, 2009, pp.1137-1146.

[15] Kim, P, Seok, J, "Bifurcation Analysis on the Hunting Behavior of a Dual-Bogie Railway Vehicle Using the Method of Multiple Scales", J. Sound Vib, Vol.32, No.9, 2010, pp.4017-4039.

[16] Polach,O, "Influence of Wheel/Rail Contact Geometry on the Behavior of a Railway Vehicle at Stability Limit", Proceedings of the ENOC-2005, Eindhoven University of Technology, The Netherlands 2005, 7-12Aug, pp.2203-2210.

[17] T.Ohji, S.C.Mukhopadhyay, M.Iwahara and S.Yamada, "Permanent Magnet Bearings for Horizontal and Veryical Shaft Machines - A Comparative Study", Journal of Applied Physics, Vol. 85, No. 8, pp 4648-4650, April 1999.

[18] Kaiser, I, Popp, K, "Interaction of Elastic Wheel set and Elastic Rails: Modeling and Simulation", Veh Syst Dyn, Vol.44, No.5, 2006, pp.932-939.

[19] T.Ohji, S.C.Mukhopadhyay, M.Iwahara and S.Yamada, "Performance of Repulsive Type Magnetic Bearing System under Nonuniform Magnetization of Permanent Magnet", IEEE Transactions on Magnetics, Vol. 36, No. 5, pp. 3696-3698, September 2000.

[20] Zhai. W, and Wang. K, "Lateral Hunting Stability of Railway Vehicle Running on Elastic Track Structures", J Comput Nonlinear Dyn 2010, 21(5):41-59.

[21] Luo. Feng, "A comprehensive survey of vision based vehicle intelligent front light system", International Journal on Smart Sensing and Intelligent Systems, vol.5, No.2, 2014, pp.701-723.

Appendix

Notation

a half lateral distance of the wheel-rail contact points

d_p half lateral span distance of the primary suspension

d_s half lateral span distance of the secondary suspension

l half fixed distance of the vehicle

b half fixed distance of the bogie

r_0 rolling radius of the wheel

h_{cs} height from the center of gravity of the vehicle to the secondary suspension

h_{bp} height from the center of gravity of the frame to the primary suspension

h_{bs} height from the center of gravity of the bogie to the secondary suspension

H_c height from the center of gravity of the empty vehicle body to the track surface

H_b height from the center of gravity of the frame to the track surface

M_c empty vehicle body mass

M_b bogie mass

M_w wheel set mass

M_{zb} rotary arm axis box mass

I_{cx} rolling inertia of the vehicle body

I_{cy} pitch inertia of empty vehicle body

I_{cz} yaw inertia of the vehicle body

I_{bx} rolling inertia of the frame

I_{by} pitch inertia of the frame

I_{bz} yaw inertia of the frame

I_{wx} rolling inertia of the wheel set

I_{wy} pitch inertia of the wheel set

I_{wz} yaw inertia of the wheel set

I_{zbx} rolling inertia of the rotary arm axis box

I_{zby} nodded inertia of the rotary arm axis box

I_{zbz} yaw inertia of the rotary arm axis box

K_{px} longitudinal stiffness of the primary suspension

K_{py} lateral stiffness of the primary suspension

K_{pz} vertical stiffness of the primary suspension

K_{sx} longitudinal stiffness of the secondary suspension

K_{sy} lateral stiffness of the secondary suspension

K_{sz} vertical stiffness of the secondary suspension

C_{pz} vertical damper of the primary suspension

C_{sy} lateral damper of the secondary suspension

C_{sz} vertical damper of the secondary suspension

c_0 unloading velocity of the anti-yaw damper

F_0 unloading force of the anti-yaw damper

y_w lateral move displacement of the wheel set

y_b lateral move displacement of the bogie

y_c lateral move displacement of the vehicle body

ϕ_b rolling angle of the bogie

ϕ_c rolling angle of the vehicle body

ψ_w yaw angle of the wheel set

ψ_b yaw angle of the bogie

ψ_c rolling angle of the vehicle body

F_{lat} resultant lateral force of wheel set due to wheel-rail contact interaction

M_{yaw} resultant yaw torque of wheel set due to wheel-rail contact interaction